

# Experimental Demonstration of Panchratnam's Phase using a Mach-Zehnder Interferometer

Sagar Prakash Barad

sagar.barad@niser.ac.in

School of Physical Sciences, NISER Bhubaneswar

April 24, 2024

## Abstract

This experiment aims to explore the dynamic evolution of geometric phase in polarized light over time. Our approach is guided by the principle that the accumulation of geometric phase is proportional to half the solid angle enclosed by a closed trajectory on the Poincaré sphere. To achieve this, we manipulate the polarization state of light using an array of optical elements, effectively serving as a geometric phase generator. We employ a Mach-Zehnder interferometer to measure both the fringes and the titular geometric phase. This involves comparing the interferometer spectrum with that of a reference wave, whose frequency matches that of the dynamical waveplate's fast axis. Additionally, we discuss various attempts made to filter the noisy data obtained using lock-in amplification. Finally, we explore several avenues for extending this project to yield improved results and showcase new ideas.

## Contents

|          |  |           |
|----------|--|-----------|
| <b>1</b> | <b>Introduction</b>                              | <b>2</b>  |
| <b>2</b> | <b>Theory</b>                                    | <b>3</b>  |
| 2.1      | Berry's Phase for a spin-1/2 system . . . . .    | 3         |
| 2.2      | Poincare Sphere . . . . .                        | 4         |
| 2.3      | Working Principle of Lock-in Detection . . . . . | 5         |
| 2.4      | Fast Fourier Transform (FFT) . . . . .           | 6         |
| 2.5      | Our Experiment . . . . .                         | 6         |
| 2.5.1    | Geometric Phase Generation . . . . .             | 8         |
| 2.5.2    | Reference Frequency Generation . . . . .         | 9         |
| <b>3</b> | <b>Experimental Setup</b>                        | <b>10</b> |
| 3.1      | Rotating half-wave plate . . . . .               | 11        |
| 3.2      | Oscilloscope Interface . . . . .                 | 11        |

|          |  |           |
|----------|--|-----------|
| <b>4</b> | <b>Attempted Improvement</b>                           | <b>12</b> |
| 4.1      | Lock-in Detection . . . . .                            | 12        |
| 4.1.1    | Attempt with TeachSpin’s Lock-in Amplifier: . . . . .  | 12        |
| 4.1.2    | Attempt with FPGA-Based Equipment (Moku:Go): . . . . . | 12        |
| 4.1.3    | Attempt with SRS-830 Lock-in Amplifier: . . . . .      | 12        |
| 4.1.4    | Development of Analytical Lock-in Detector: . . . . .  | 13        |
| 4.2      | Tuning Geoemetric Phase Range . . . . .                | 13        |
| <b>5</b> | <b>Observations and Analysis</b>                       | <b>14</b> |
| 5.1      | high ( $> 10$ Hz) frequency regime . . . . .           | 14        |
| 5.2      | Low ( $< 10$ Hz) frequency regime . . . . .            | 14        |
| <b>6</b> | <b>Conclusions</b>                                     | <b>14</b> |
| <b>7</b> | <b>Future Work</b>                                     | <b>16</b> |

## 1 Introduction

In quantum mechanics, states that differ solely due to a dynamical phase are deemed indistinguishable, maintaining a norm-squared of one and leaving probability distributions unchanged. In contrast, the geometric phase emerges from the geometry of the path traced by a quantum state in parameter space (e.g., the Bloch sphere in a two-level quantum system). Now the concept of geometric phase, was introduced by Sir Michael Berry in 1983[1]. Berry’s work, often referred to as the Berry Phase, revealed that when a quantum system undergoes adiabatic changes in its parameters—changes that occur slowly and smoothly—a phase factor is acquired by the system’s wave function. The geometric phase differs from the dynamical phase due to its lack of universal dependence on a global phase, making it non-normalizable in most cases. This theoretical breakthrough has far-reaching implications, particularly in optics and condensed matter physics. Specially in the field of optics, the geometric phase is closely associated with the polarization of light, which has led to innovations such as geometric phase holograms. In condensed matter physics, it has proven instrumental in explaining phenomena like the Aharonov-Bohm effect and offering insights into topological insulators.

For a two-level quantum system, the geometric phase is precisely half the solid angle covered by the state’s trajectory during its temporal evolution at the core of the Bloch sphere. This distinct property not only underscores the non-normalizability of the geometric phase but also opens avenues for experimental measurements. Unlike its dynamical counterpart, the geometric phase’s resistance to normalization makes it tangible and, most importantly, measurable in an experimental setting. This experiment aims to study the temporal evolution of the geometric phase in polarized light. Our approach involves manipulating the polarization state to create a closed trajectory on the Poincaré sphere[2]. The dynamics of this trajectory result in the accumulation of a geometric phase, precisely half the solid angle enclosed by the trajectory on the sphere’s center. Inspired by the work of [3], we aim to replicate their findings, showcasing that a dynamic alteration in the geometric phase of light induces a frequency shift. Additionally, we explore scenarios where the geometric phase changes linearly with time, leading to corresponding variations in the frequency of the light.

The experimental setup, detailed in accompanying figures, facilitates the observation of these phenomena. A critical aspect of this experiment is the measurement of the frequency shift induced by the changing geometric phase. For this purpose, a Mach Zander Interferometer is used, with details of its setup to be discussed in the subsequent section. We will deal with interference of light beams with different frequencies but the same amplitude, simplifying assumptions for the sake of clarity. The resulting beat frequency from the interferometer allows for the observation and measurement of the frequency shift, providing valuable insights into the dynamic relationship between geometric phase changes and corresponding frequency alterations in polarized light.

## 2 Theory

In this section we discuss the equivalence between the dynamics of a two-level quantum system on a Bloch sphere and the Poincare sphere of light polarisation. We begin with the discussion of geometric phase for the most general quantum system undergoing an adiabatic evolution.

Consider a quantum system described by the Hamiltonian  $H(\vec{R})$ , where  $\vec{R}$  are a set of parameters of the phase space that the Hamiltonian depends on. Suppose the dynamics of the system is such that the parameter  $\vec{R}(t)$  changes adiabatically as a function of time. The time evolved wave-function is then obtained by solving the Schrodinger equation

$$H(\vec{R}) |\Psi(t)\rangle = \iota \frac{d}{dt} |\Psi(t)\rangle. \quad (1)$$

We assume that the system at  $t = 0$  is in some eigenstate  $|n\rangle$  of  $H(\vec{R})$  with eigenvalue  $E_n$ . We may assume that the system remains in this eigenstate under adiabatic evolution. We use the following ansatz for solving the Schrodinger equation

$$|\Psi(t)\rangle = \exp\left(\iota\eta(t) - \iota \int_0^t E_n(\vec{R}_s) ds\right) |n, \vec{R}(t)\rangle. \quad (2)$$

Substituting the ansatz in the Schrodinger equation we obtain an expression for  $\eta(t)$

$$\eta(t) = \iota \int_{\vec{R}(0)}^{\vec{R}(t)} \langle n, \vec{R} | \nabla_{\vec{R}} |n, \vec{R}\rangle d\vec{R}. \quad (3)$$

This  $\eta(t)$  is called the Berry's phase which is a real quantity. This phase is accumulated in addition to the dynamical phase that is accumulated (the integral in the exponential present in the ansatz is the dynamical phase). While the dynamical phase accumulated by a quantum system has no physical significance (which is to say that no experiment can experimentally detect such a phase). The Berry's phase has physical consequences that can be experimentally probed.

### 2.1 Berry's Phase for a spin-1/2 system

A spin-1/2 system is one of the simplest examples of a two-level quantum system. In this section we discuss this system and compute the geometric phase for a certain special kind of time evolution. The system is governed by the Hamiltonian

$$H(\vec{R}) = k \vec{S} \cdot \vec{R} \quad (4)$$

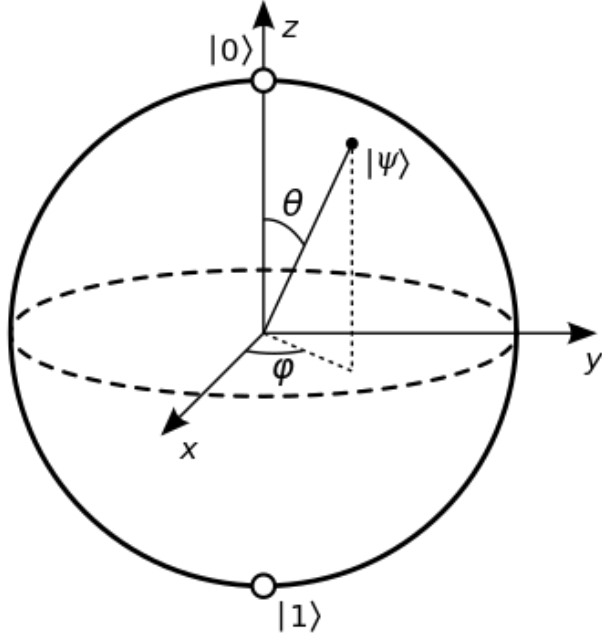


Figure 1: The schematic diagram of a Bloch sphere the relative position of different states are arbitrary.

where  $k$  is a constant. This is a Hamiltonian for the spin-1/2 particle in a magnetic field the constant absorbs the magnetic moment and the fundamental constants. If the two levels of a two-level quantum system are labelled as  $|+\rangle$  and  $|-\rangle$  their dynamics can be represented on the Bloch sphere as shown in 1. For adiabatic evolutions such that the trajectory traced by the Bloch vector on the Bloch sphere is closed the geometric phase accumulated through the trajectory is given by

$$\eta = \frac{\Omega}{2} \quad (5)$$

where  $\Omega$  is the solid angle subtended by the surface formed by the closed trajectory on the Bloch sphere.

## 2.2 Poincare Sphere

The polarisation of an electromagnetic wave is the quantity the describes the geometry and orientation of electric field oscillations. To state the polarisation of a wave we need four real numbers or two complex numbers, these are called the Stokes parameters. The Stokes vector has the Stokes parameters as its components. The evolution of Stokes vector can be represented on a sphere. This sphere is called the Poincare sphere (shown in 2). The Bloch and the Poincare sphere are equivalent in the sense that any state on one can be mapped to the other. Also we can construct a Hamiltonian to mimic any changes in the polarisation state of light, similarly we can do specific polarisation changes to mimic the dynamics of any time-dependent Hamiltonian. So the properties true for dynamics on a Bloch sphere is also true for the dynamics on a Poincare sphere.

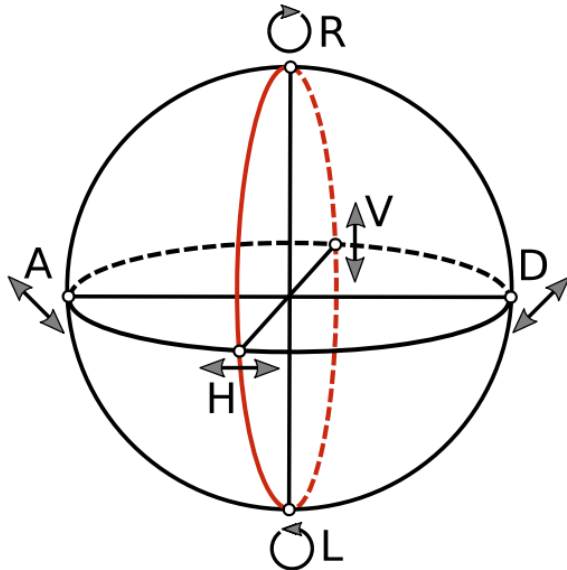


Figure 2: The schematic diagram for the Poincaré sphere the points labelled by H, L, R and V are horizontally, left-circularly, right-circularly and vertically polarized respectively. The other two polarizations on the equatorial plane are diagonal. On the remaining part of the sphere we see elliptically polarised light. On the equator we see linearly polarised light.

### 2.3 Working Principle of Lock-in Detection

Lock-in detection is a powerful technique used in signal processing to extract signals that are buried in noise. At its core, it relies on the principle of modulating the signal of interest and then demodulating it using a reference signal. The lock-in amplifier operates by multiplying the input signal by the reference signal and then integrating the result over a specific time interval. Mathematically, the lock-in detection process can be described as follows. Let  $S(t)$  be the input signal and  $R(t)$  be the reference signal. The output of the lock-in amplifier  $V_{out}$  is given by:

$$V_{out} = \int_0^T S(t) \cdot R(t) dt \quad (6)$$

where  $T$  is the integration time.

The reference signal is typically chosen to be a sine wave due to its orthogonal properties and its ability to easily synchronize with the input signal. The use of a sine wave reference ensures that the lock-in amplifier is sensitive only to the component of the input signal that is in phase with the reference signal, effectively filtering out noise and other unwanted components. When using a reference signal that is not a sine wave, such as a square wave or a triangle wave, it is necessary to convert it to a sine wave using a function generator or other signal processing techniques. This conversion ensures that the reference signal maintains its phase relationship with the input signal, enabling effective signal extraction through lock-in detection.

## 2.4 Fast Fourier Transform (FFT)

The Fast Fourier Transform (FFT) is a widely used algorithm in digital signal processing for efficiently computing the Discrete Fourier Transform (DFT) of a sequence of data points. It reduces the computational complexity of the DFT from  $O(N^2)$  to  $O(N \log N)$ , where  $N$  is the number of data points.

Mathematically, the DFT of a sequence  $x[n]$  of length  $N$  is defined as:

$$X[k] = \sum_{n=0}^{N-1} x[n]e^{-j2\pi kn/N}, \quad k = 0, 1, \dots, N - 1 \quad (7)$$

The FFT algorithm breaks down this computation into smaller subproblems by exploiting the periodicity and symmetry properties of the complex exponential terms in the DFT formula. By recursively dividing the input sequence into smaller sub-sequences and applying the FFT to each sub-sequence, the FFT algorithm achieves significant computational savings. The FFT algorithm is particularly efficient for sequences with a length that is a power of 2, although extensions and optimizations exist for other lengths as well.

The output of the FFT represents the frequency-domain representation of the input signal, with  $|X[k]|$  representing the magnitude and  $\angle X[k]$  representing the phase at each frequency bin  $k$ . In practice, the FFT is widely used in applications such as signal analysis, filtering, spectral estimation, and convolution, owing to its computational efficiency and accuracy.

## 2.5 Our Experiment

In this section we describe our experiment in which we seek to observe an effect of geometric phase changing with time. We keep the following two things in mind

1. The dynamics of polarisation of light on a Poincare sphere, such that the trajectory of evolution is closed, will accumulate a geometric phase which equals half the solid angle subtended by the surface enclosed by the closed trajectory on the center of the sphere.
2. When the dynamics is such that the geometric phase is changing with linearly with time, the frequency of light changes. We do not discuss the theoretical basis of this in our report.
3. We use a portion of our beam to generate a reference square signal with the same frequency as the rotator responsible for generating the geometric phase.

So here's what we need to do

1. Change the polarisation state of light such that its representation on the Poincare sphere forms a closed trajectory.
2. Ensure that the solid angle subtended by the surface enclosed by the closed trajectory changes with time.
3. And have a setup such that the change in frequency of the light beam which accumulates the geometric phase can be observed.

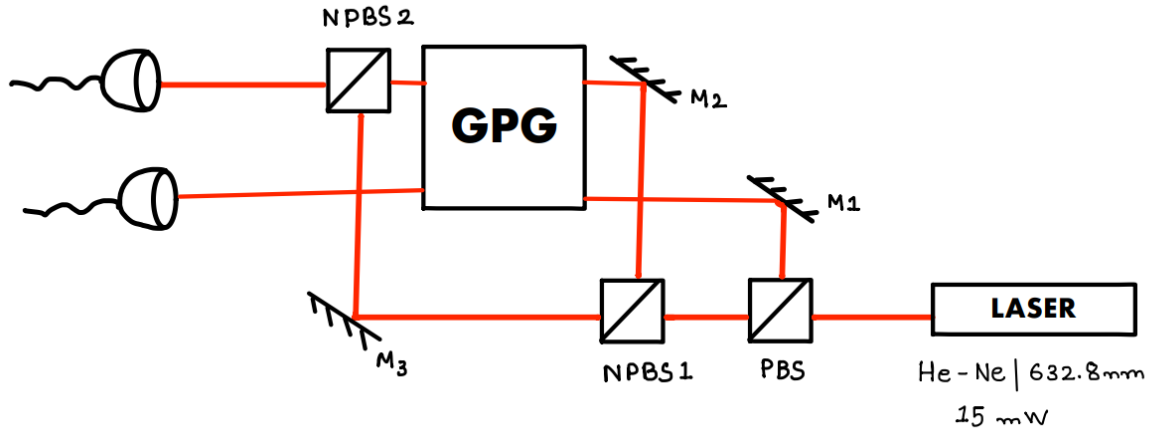


Figure 3: The experimental setup involves an optics configuration designed for measuring the phase shift resulting from dynamical geometric phase. PBS refers to a polarizing beam splitter, while M represents silver-coated mirrors reflecting 100% of light.  $NPBS_1$  and  $NPBS_2$  denote non-polarizing beam splitters, and  $D_1$  and  $D_2$  are the photodiodes used to detect the output intensity.

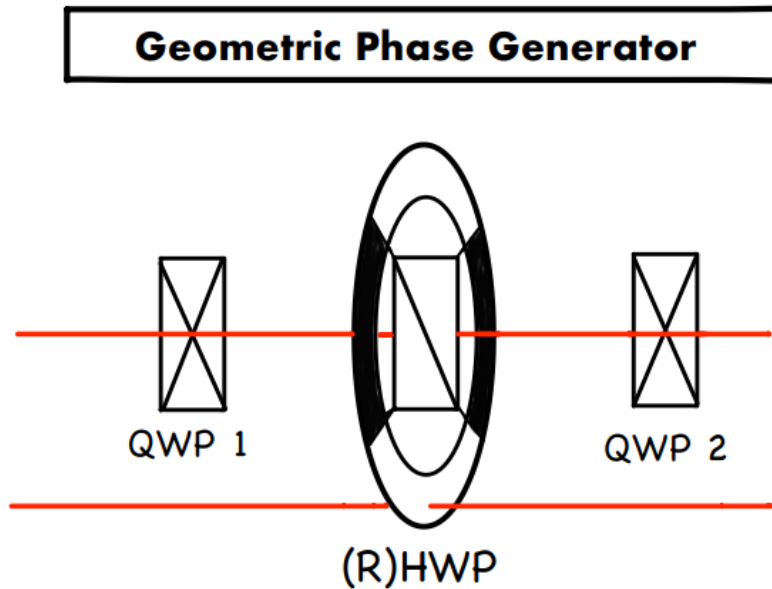


Figure 4: The Geometric Phase Generator consists of an array of optical elements responsible for modulating the polarization of waves. Namely, it has two quarter-wave plates,  $QWP_1$  and  $QWP_2$ , and a rotating half-wave plate,  $(R)HWP$ , which is attached to a fidget spinner-like rotator in the middle. This rotator can be strategically blocked and rotated at desired angular velocities.

### 2.5.1 Geometric Phase Generation

We achieve the above goals with the optical setup shown in Figure 3. The corresponding evolution on the Poincaré sphere is shown in Figure 5. We now justify how the experimental setup leads to the shown trajectory on the Poincaré sphere.

1. The unpolarized light from the laser is first passed through a PBS oriented such that the transmitted light is horizontally polarized (H) and the reflected light is vertically polarized (V). The transmitted beam enters the Mach-Zander setup so that we begin the evolution at point H on the sphere.
2. The horizontally polarized beam is then split into two. The beam splitter does not change the polarization state of the light. So the light on both arms is horizontally polarized.
3. The light in the arm containing M1 undergoes no change in its polarization state. This will serve as the reference beam from which the changes in frequency will later be measured.
4. The light in the arm containing M2 is initially horizontally polarized. But it is subjected to an array of quarter wave-plates and one rotating half-wave plate, which we call the geometric phase generator. The first quarter wave-plate is kept at an axis making an angle of  $\pi/4$  from its fast axis horizontal, so the horizontally polarized light is transformed into right circularly polarized light. Thus, the Stokes vector moves from H to RC on the sphere.
5. Then the light is passed through a rotating half wave-plate at any time making an angle  $3\pi/4 + \phi$  with the horizontal. The angle  $\phi$  varies with time (as we rotate the wave-plate with a motor). This wave-plate changes the right circularly polarized light to left circularly polarized but with an offset angle  $2\phi$ . So the light beam is moved from RC to LC on the sphere.
6. Now the light is passed through a quarter wave-plate kept at an axis making an angle of  $\pi/4$  from its fast axis horizontal or basically parallel to the orientation of the first quarter wave plate. Here the beam is transformed from left circularly polarized light with accumulated phase to horizontally polarized light with an accumulated phase of  $2\phi$ .
7. The trajectory HRCLCH is a closed trajectory on the Poincaré sphere. This implies the beam accumulates a phase difference that is equal to half the solid angle subtended by the surface enclosed by the trajectory at the center of the sphere.

Horizontally polarized light ( $|H\rangle$ ) can be represented as  $\begin{pmatrix} 1 \\ 0 \end{pmatrix}$ .

$$\begin{pmatrix} 1 \\ 0 \end{pmatrix} \xrightarrow{\text{QWP at } 45^\circ} \begin{pmatrix} \cos\left(\frac{\pi}{4}\right) \\ i \sin\left(\frac{\pi}{4}\right) \end{pmatrix} \xrightarrow{\text{HWP at } \frac{\pi}{2} + \phi} e^{-2i\phi} \begin{pmatrix} \cos\left(\frac{\pi}{4}\right) \\ -i \sin\left(\frac{\pi}{4}\right) \end{pmatrix} \xrightarrow{\text{QWP at } 45^\circ} e^{-2i\phi} \begin{pmatrix} 1 \\ 0 \end{pmatrix}$$

So these two waves can and will interfere:

$$E = E_0 + E_0 e^{-2i\phi} \quad (2.1)$$

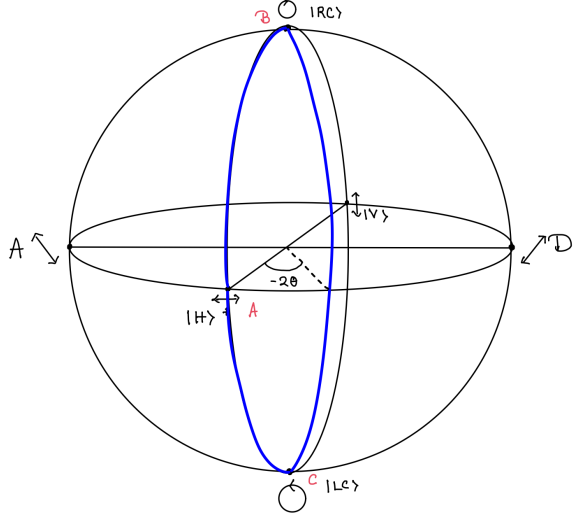


Figure 5: The trajectory followed by the Stokes vector on the Poincare sphere. In our setup the light goes from H to RC to LC and back to H during one traversal of the setup.

and the resulting intensity, which depends on  $|E|^2$ , can be expressed as

$$|E|^2 = 2E_0^2(1 + \cos(2\phi)).$$

The solid angle subtended by a surface on a sphere at the center of the sphere is given by

$$\Lambda = \int \int_S \frac{\hat{r} \cdot \hat{n}}{r^2} dS \quad (8)$$

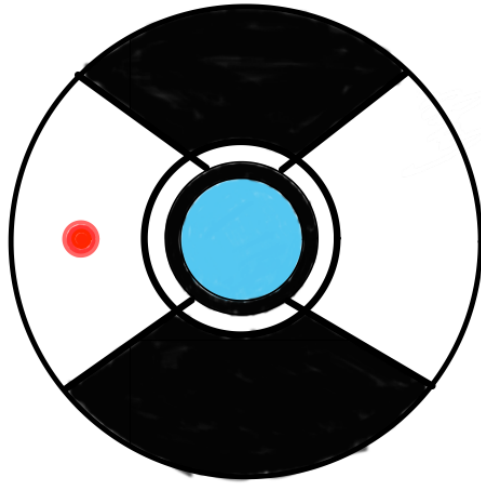
in our case the solid angle is

$$\Lambda = 4\phi. \quad (9)$$

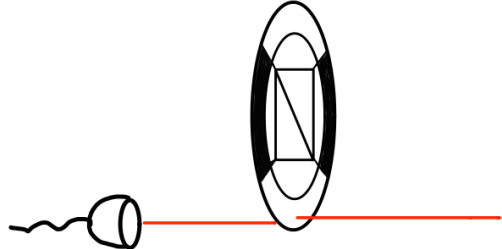
Suppose the axis of the second quarter wave-plate is rotated with an angular velocity  $\Omega = d\phi/dt$ , then the arc RBL on the Poincare sphere moves away from the arc RHL with an angular velocity of  $2\Omega$ . So the geometric phase  $\phi$  changes with time as  $\psi = \psi_0 + 2\Omega t$ .

### 2.5.2 Reference Frequency Generation

For the task of creating a reference signal, we utilize the same Rotating Half-Wave Plate (RHWP) by covering 1/4th of its area at diametrically opposite points (see figure 7). We then direct the reflected portion of light from the initial Polarizing Beam Splitter (PBS) towards the RHWP and finally to a detector. This setup enables the generation of a square wave signal with a frequency that is twice that of the rotating frequency of the spinor ( $2\Omega$ ). The RHWP, with its adjustable rotation, serves as a convenient means to modulate the light intensity, thereby producing the desired square wave output.



(a) The Half Wave Plate Rotator is stategically blocked half of the time during rotation, with the half-wave plate (*HWP*) positioned at the center.

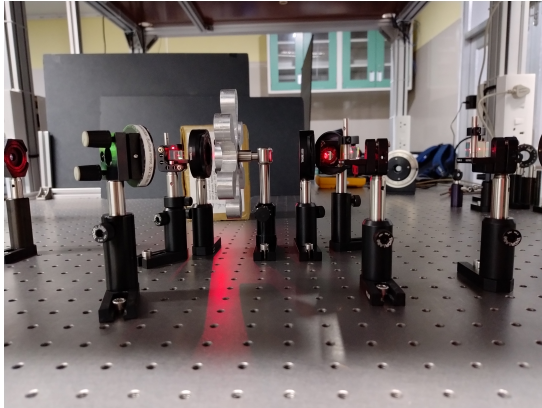


(b) Periodic blocking the laser to achieve a square wave with twice the rotating frequency, i.e., the frequency of the rotator.

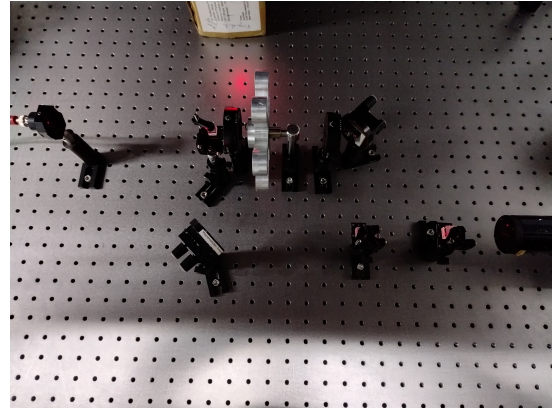
Figure 6: Generation of reference signal with same frequency as of the rotating half-wave plate.

### 3 Experimental Setup

In this section, we discuss the realization of our experimental setup. To observe the frequency shift through beats, we set up a Mach-Zander interferometer with wave plates in two of its arms. We provide the labeled image of the experimental setup in Figure 5. Figure 6 shows an image of the rotating half-wave plate, and Figure 7 shows the detector setup.



(a) Side view of the experimental setup.



(b) Top view of the experimental setup.

Figure 7: Mach Zander Interferometer with a rotating half-wave plate.

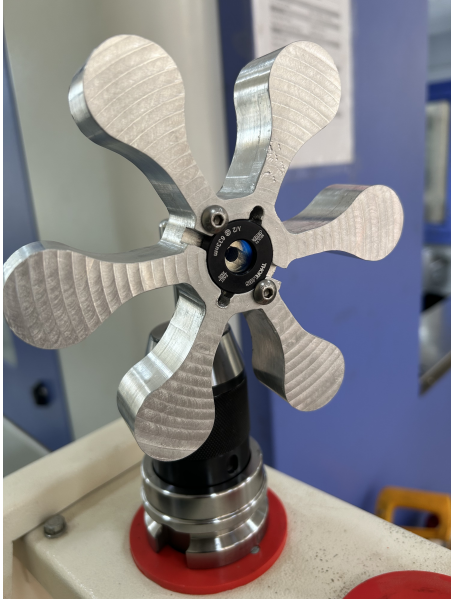


Figure 8: Rotator with a shape of a fidget spinner, having a half-wave plate fixed in the middle.

### 3.1 Rotating half-wave plate

Between the first quarter-wave plate (QWP 1) and the second quarter-wave plate (QWP 2), we have integrated a rotating half-wave plate capable of smooth and controlled rotations. This precision setup essentially resembles a fidget spinner, with counterweights in each of its six arms and a half-wave plate placed in the middle. The fidget spinner design ensures stability and balanced rotation. Fidget spinners utilize ball bearings or low-friction materials to reduce friction and allow for extended spin times. In our setup, we will provide torque to one of its arms, and with appropriate torque, we will achieve 5 to 6 seconds of constant sustained rotations of the wave plate. This integration of the fidget spinner-inspired design enhances the stability and endurance of our experimental setup, allowing for prolonged and consistent rotation of the half-wave plate. Additionally, we have blocked portions of the detector and passed a light signal through it to obtain the desired signal.

### 3.2 Oscilloscope Interface

For measurements, we utilized a mounted Silicon photodiode with the cathode grounded, specifically the SM1PD1A model from Thorlabs. To ensure proper impedance matching, we connected a  $50\Omega$  terminus to the BNC cable linking the photodiode to the oscilloscope. Inadequate impedance matching between the photodiode and the oscilloscope's input impedance can lead to signal distortion due to reflections. Without employing the terminus, we were unable to accurately capture fluctuations in the output of the interferometer caused by external perturbations. Essentially, the  $50\Omega$  terminus acts as a resistor connected across the input terminals of the oscilloscope. A similar setup has been used for capturing the reference signal.

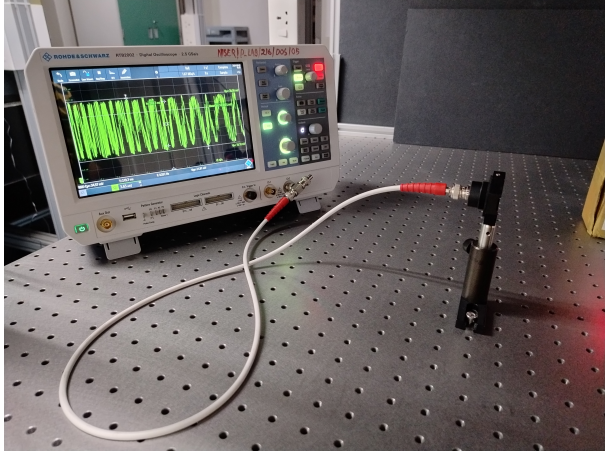


Figure 9: Setup for detecting the interference of two waves using a photodiode and oscilloscope.

## 4 Attempted Improvement

In our experimental setup, we encountered significant noise in the data due to the wobbling of the waveplate spinner during rotation. This noise, nearly as large in amplitude as the signal itself, posed a considerable challenge in obtaining accurate measurements. To address this issue, we attempted various methods of lock-in detection, each with its own set of challenges and limitations.

### 4.1 Lock-in Detection

#### 4.1.1 Attempt with TeachSpin's Lock-in Amplifier:

Initially, we tried utilizing TeachSpin's lock-in amplifier. Given that we had a square wave reference signal, we needed to convert it to a sine wave for proper lock-in detection. Although the amplifier offered an option for this conversion, we found that the square input was converted to a distorted sine wave, rendering it unsuitable for effective lock-in detection.

#### 4.1.2 Attempt with FPGA-Based Equipment (Moku:Go):

In our next attempt, we turned to an FPGA-based equipment, specifically Moku:Go, which was already configured to function as a lock-in amplifier. This equipment featured an internal square wave to sine wave converter using a phase lock-loop. However, upon inspecting just the output of the phase lock-loop, we discovered that it was not functioning properly, hindering our lock-in detection efforts.

#### 4.1.3 Attempt with SRS-830 Lock-in Amplifier:

We also experimented with the SRS-830 lock-in amplifier. However, we encountered difficulties in locking the signal due to its low frequency. The SRS-830 could only effectively lock onto signals with frequencies higher than 10 Hz. Since the frequency of our spinner reached a maximum of 13 Hz but quickly damped to zero within approximately 90 seconds, the SRS-830 was unable to maintain lock-in detection for the desired duration.

#### 4.1.4 Development of Analytical Lock-in Detector:

Additionally, another group of students worked on developing a lock-in detector tailored to our setup. Their approach involved performing Fourier transforms of both the signal and reference to extract frequencies and then analytically computing the resultant amplitude. While this method provided accurate results, it lacked real-time detection capability, which was essential for our experiment as the signal frequency decayed over time.

Despite our attempts, achieving effective lock-in detection proved to be a significant challenge due to the dynamic nature of our experimental setup and the limitations of available equipment. Further exploration and refinement of detection methods may be necessary to overcome these obstacles and obtain accurate measurements in the presence of noise.

## 4.2 Tuning Geoemetric Phase Range

In our current experimental scheme the geometric phase accumulated changes from  $0-2\pi$  upon one rotation of the waveplate spinner. In this case the amplitude of the signal is maximum. However, if we were to design a setup where the range of the geometric phase is  $[0, \theta]$  then the amplitude of the signal would take a value between 0 and the maximum, depending on the  $\theta$  value. A linear amplitude vs  $\theta$  plot would then ascertain the observed phase as the geometric phase.

Designing this setup is not easy at all. First of all we have to think of a suitable polarisation space geometry that we want to implement experimentally. After this even though there are methods for realising any trajectory in phase space using an arbitrary number of waveplates with different thicknesses we need to come up with a practical array of waveplates that does the job.

A nice geometry that we could think of started with the polarisation vector at some elliptical polarisation with  $\theta = 0$  and  $\phi = \phi_0$  (say), we then go to right circularly polarised light (we could also go to left circularly polarised light), and from there we transform back to another elliptically polarised light on the same latitude as the initial polarisation vector i.e. with  $\theta = \theta'$  and  $\phi = \phi_0$ , from this state we can go back to the initial state by a halfwave plate. To realise this trajectory the dynamical waveplate should be such that it takes light from circular polarisation to some elliptical polarisation with same  $\phi$  but different  $\theta$  depending on the angle its fast axis makes with the horizontal. We could not come up with a set of waveplates that does this. We tried quite a few things, from increasing the number of waveplates to upto five to introducing the possibility of rotating more than one waveplate but nothing we tried seem to work.

We should highlight in what ways the current scheme is special and why is it so difficult to come up with similar schemes. The special part of the current experimental scheme is that from circularly polarised light we come back to the equator i.e.  $\phi = 0$  this is latitude is special because no matter where you are you can always go to circular polarisation from a waveplate aligned at a constant angle. No other latitude has this property. This problem seems to vanish if we could have waveplates whose axis change in time but then different waveplates are required to spin in different ways and their motion will have to synchronised.

There can be other geometries that do the job but it should be kept in mind that the geometry should not be too complicated because in case of complicated geometries, say in case the polarisation vector forms two closed loops, the computation of geometric phase would be ambiguous.

## 5 Observations and Analysis

In our previous report, we demonstrated various aspects of our experiment. Firstly, we observed noise in the signal resulting from external perturbations, with similar noise attributed to the wobbling of the spinner. Secondly, blocking one arm of the interferometer resulted in the absence of signal oscillations. Thirdly, with both arms unblocked but the waveplate stationary, we observed a slightly unstable signal, characteristic of interference. Lastly, rotation of the waveplate induced changes in the signal.

For the observation, we will analyze the intensity spectrum for both the input and reference signals. We will perform FFT analysis for both profiles and extract the dominant frequencies for each signal. It's important to note that the reference signal is expected to be at  $2\Omega$ , where  $\Omega$  represents the rotating frequency of the half-wave plate (HWP) at a rate of ( $R$ ) rotations per second. We anticipate that the input signal rotates at twice the frequency of the rotating frequency, implying that both signals should exhibit the same frequency in the FFT analysis.

### 5.1 high ( $> 10$ Hz) frequency regime

The results, depicted in Figure 9, reveal an excellent match in the dominant frequency between both the reference and signal beams across all cases. This confirms that the observed signal indeed arises from geometric phase accumulation. We specifically focus on data from the high frequency regime to ensure that the effect of wobbling on the spinner's motion remains negligible. Additionally, at higher frequencies, the damping of frequency is slow relative to the spinner's rotations, allowing for a larger number of oscillations at nearly the same frequency.

### 5.2 Low ( $< 10$ Hz) frequency regime

Figure 10 displays the results, where, notably, the dominant frequency did not consistently align across all cases. This outcome was somewhat anticipated, given that at lower frequencies, the spinner undergoes fewer rotations and experiences more pronounced wobbling. Consequently, the frequency variation over time becomes more discernible. Additionally, the wobbling induces erratic fluctuations in the spinner's rotational motion. The Fourier analysis unequivocally confirms the alignment of the dominant frequency between the signal and the acquired reference beam. This alignment strongly suggests the presence of geometric phase within the system.

Results and the data analysis are available in this [Github](#) link.

## 6 Conclusions

We have successfully illustrated the generation and measurement of geometric phase in light using a Mach-Zehnder interferometer. Validating this phenomenon, we compare the Fourier spectrum of our signal with that of a reference square wave, establishing an analytical link between geometric phase and the area enclosed by the light wave trajectory in polarization space. While our comparison confirms the presence of dynamical geometric phase, our signal is marred by significant noise. This noise primarily arises from the high-frequency contributions stemming from the wobbling of our waveplate spinner. Despite our attempts at noise reduction through lock-in amplification, technical challenges impede

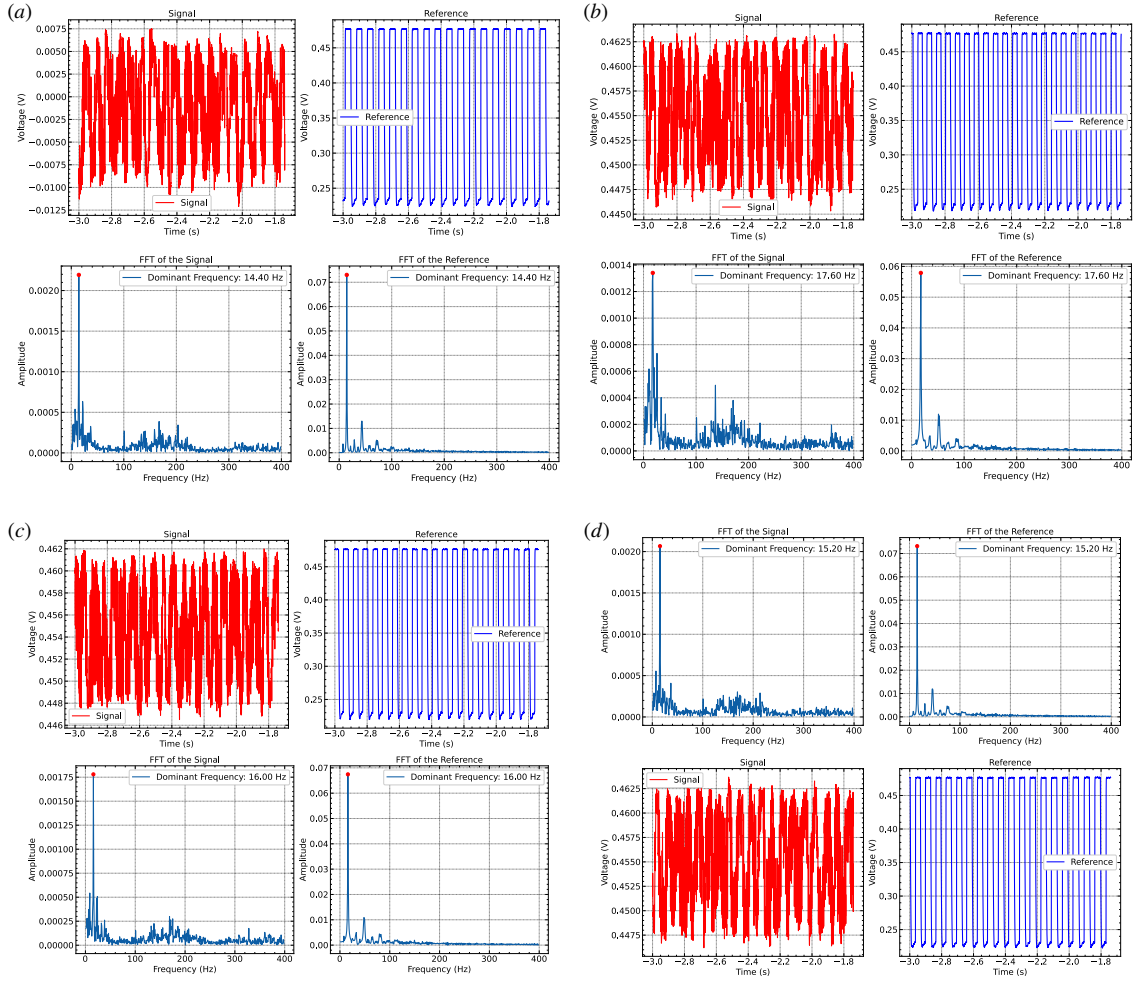


Figure 10: The signal, reference and their corresponding Fourier spectra for high frequencies. In all (a)-(d) be see that the dominant frequency for both the signal and the reference is exactly the same.

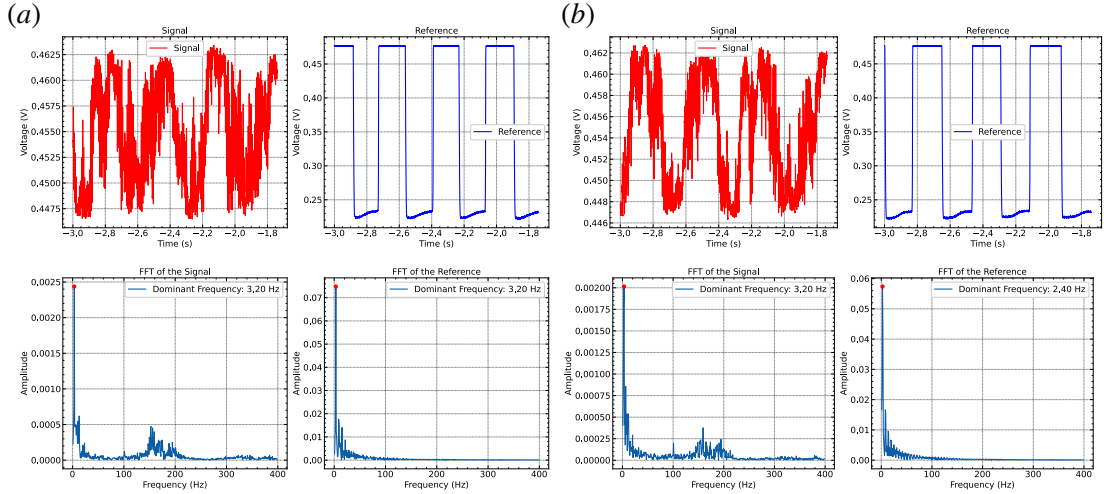


Figure 11: The signal, reference and their corresponding Fourier spectra for low frequencies. While the dominant frequencies match in (a), they do not match in (b).

our progress, particularly in converting the square wave to a sine wave and dealing with the low signal frequency. Efforts to devise a new experimental setup to modulate the range of accumulated geometric phase have proven unsuccessful thus far. Though theoretically possible to navigate any trajectory in polarization space using an array of waveplates with varying thickness and fast axis angles, practical implementation remains elusive.

Exploring alternative approaches, such as substituting our spinner with a motor, presents a viable solution. However, interfacing issues between the motor driver and Arduino hinder our ability to execute this strategy effectively. The precise root of these interfacing challenges remains unclear, necessitating further investigation.

Thus, our experimental findings confirm the existence of geometric phase accumulation, mitigating noise and devising versatile experimental setups pose ongoing challenges. Addressing these obstacles requires innovative problem-solving and thorough exploration of technical solutions.

## 7 Future Work

The task at hand involves tuning the range of the geometric phase in an experimental setup, aiming to extend it from the standard  $0$  to  $2\pi$  to a custom range of  $0$  to  $\theta$ . This adjustment necessitates a thoughtful design to control the amplitude of the signal within this new phase range. The challenge begins with selecting an appropriate polarization space geometry. One proposed trajectory involves transitioning from elliptical to circular polarization, then returning to elliptical polarization on the same latitude, and finally reverting to the initial state using a half-wave plate. However, realizing such a trajectory proves daunting, as it requires precise manipulation of waveplates. Despite attempts with various configurations, including multiple waveplates and adjustments in their orientation, achieving the desired trajectory remains elusive. The current experimental scheme's uniqueness lies in its ability to return to the equatorial plane from circular polarization,

simplifying manipulation compared to other latitudes. However, replicating this simplicity in alternative schemes proves challenging, primarily due to the need for synchronized motion of multiple waveplates. Complexity in waveplate arrangements must be minimized to prevent ambiguity in phase calculations. Overly intricate geometries, such as those forming multiple closed loops, can obscure the computation of the geometric phase.

Hence, designing an experimental setup to control the geometric phase within a specified range requires meticulous consideration of polarization trajectories and synchronization of waveplate movements. Simplifying the geometry while retaining control over the phase range is essential for accurate and unambiguous phase manipulation.

## References

- [1] S. Pancharatnam. Generalized theory of interference, and its applications. *Proceedings of the Indian Academy of Sciences - Section A*, 44(5):247–262, 1956.
- [2] C. Cisowski, J. B. Götte, and S. Franke-Arnold. Colloquium: Geometric phases of light: Insights from fiber bundle theory. *Rev. Mod. Phys.*, 94:031001, Jul 2022.
- [3] R. Simon, H. J. Kimble, and E. C. G. Sudarshan. Evolving geometric phase and its dynamical manifestation as a frequency shift: An optical experiment. *Phys. Rev. Lett.*, 61:19–22, Jul 1988.